The Astrophysical Journal Letters, 880:L13 (6pp), 2019 July 20 https://doi.org/10.3847/2041-8213/ab2f8d

Kinetic Theory of Ion Acoustic Waves Observed at Comet 67P/Churyumov–Gerasimenko

Saeed ur Rehman, Asif Shah, and Qamar ul Haque
Theoretical Physics Division, PINSTECH, Nilore Islamabad 44000, Pakistan; surehman@ualberta.ca, saeed_physics@yahoo.com
Received 2019 March 29; revised 2019 July 3; accepted 2019 July 5; published 2019 July 19

Abstract

This work presents the resonance interaction of ion acoustic waves with the cometary plasma as observed at comet 67P/Churyumov–Gerasimenko. The plasma is comprised of cold, warm, and suprathermal electron populations and water ions such that the quasineutrality is satisfied. The cold electron population is found to play a dominant role in the damping of the waves, and its maximum Landau damping rate is observed when it is 2% of the total electron density in the system. It is determined that lowering the cold electron density supports the current-driven ion acoustic instability at a relatively lower drift speed of the warm and suprathermal electron species. In the absence of cold electrons, the wave phase speed does not change by populating the high-energy suprathermal electron species, therefore, the Landau damping rate of both warm and suprathermal electrons increases by increasing their respective densities. The growth rate of the current-driven ion acoustic instability decreases by elevating the concentration of suprathermal electrons in the case of drifting warm and stationary suprathermal electrons. In the case of stationary warm and drifting suprathermal electrons, the elevated density of suprathermal electron instead favors the instability.

Key words: comets: general – planetary systems – plasmas – waves

1. Introduction

Recently, the *Rosetta* spacecraft reached the comet 67P/Churyumov–Gerasimenko (67P) after a 10 yr journey. This is a relatively weakly outgassing comet. *Rosetta* probed the cometary environment and found that the plasma there is mainly of cometary origin and mostly consists of water ions (Nilsson et al. 2015; Behar et al. 2016). The observation of suprathermal electrons along with warm electrons has also been reported (Clark et al. 2015; Madanian et al. 2016). Up to now, two possible mechanisms have been identified to produce the suprathermal electrons. One is the heating of electrons by wave–particle interaction (Broiles et al. 2016a; Karlsson et al. 2017) and the other is the acceleration of electrons due to an ambipolar electric field (Madanian et al. 2016). Deca et al. (2017) used a 3D kinetic approach to explain the physical process that results in non-thermal electron distributions. Their simulation supports the latter model. In addition to warm and suprathermal populations, a cold electron population has also been observed at comet 67P (Eriksson et al. 2017; Gilet et al. 2017; Engelhardt et al. 2018). It is suggested that the cooling of electrons by collisions with neutrals produced cold electrons there.

Broiles et al. (2016b) modeled the warm and suprathermal electrons at comet 67P by kappa distributions. The qualitative comparison of the observed and modeled differential energy flux showed an excellent agreement below 100 eV. However, the model underestimated the flux below 20 eV, which could be corrected by considering the cold electron population. Madsen et al. (2018) observed waves inside the diamagnetic cavity of comet 67P with frequencies similar to the lower hybrid waves outside the cavity by analyzing the one-dimensional electric field signals measured with the Langmuir probes on board *Rosetta*. They interpreted them as being caused by the outside lower hybrid waves.

The *International Cometary Explorer* (*ICE*) spacecraft at comet Giacobini–Zinner (Scarf et al. 1986) and the *Sakigake* spacecraft at comet Halley (Oya et al. 1986) detected ion acoustic waves. Recently, the *Rosetta* spacecraft at a distance of 28 km from the nucleus of comet 67P also observed ion acoustic waves (Gunell et al. 2017b). Gunell et al. (2017b) showed that for the observed ion acoustic waves only electrons and water ions are important, and the influence of solar wind ions is minimal and can be ignored. In the wave dispersion analysis, they modeled the electron with a single thermal distribution and did not account for the suprathermal electrons. Ion acoustic waves have also been reported inside the diamagnetic cavity (Gunell et al. 2017a) where both cold and warm electron populations are present. The authors proposed that the waves were driven by a current flowing through a filamentary extension of the cavity.

These observations motivated us to develop a comprehensive analytical model for studying ion acoustic wave dispersion and its interaction with the cometary plasma.

2. Kinetic Model

In our model, the cometary plasma is comprised of water ions H_2O^+, and warm, cold, and suprathermal electrons such that $n_{e_w} + n_{e_c} + n_{e_\kappa} = n_i$, where n_{e_w}, n_{e_c}, n_{e_κ}, and n_i are the equilibrium number densities of warm, cold, suprathermal electrons, and ion species, respectively. The unperturbed warm, cold electrons and ions are assumed to follow a three-dimensional drifting Maxwellian distribution as

$$f_\alpha(v_\alpha) = \frac{1}{(\sqrt{\pi}\, v_{t\alpha})^3} \exp\left(-\frac{(v_\alpha - u_{0_\alpha})^2}{v_{t\alpha}^2}\right). \quad (1)$$

Here v_α is the speed of α species, i.e., $\alpha = e_w,\ e_c,\ i$. $v_{t\alpha} = \sqrt{2T_\alpha/m_\alpha}$ is the thermal speed of species α with mass m_α and temperature T_α in units of energy. u_{0_α} is the drift speed of α species. The suprathermal electrons in the plasma are supposed to follow a three-dimensional drifting kappa

distribution as

$$f_{e_\kappa}(v_{e_\kappa}) = \frac{1}{(\sqrt{\pi\kappa_e}\theta_{e_\kappa})^3}\frac{\Gamma(\kappa_e+1)}{\Gamma\left(\kappa_e-\frac{1}{2}\right)} \times\left(1+\frac{(v_{e_\kappa}-u_{0_\kappa})^2}{\kappa_e\theta_{e_\kappa}^2}\right)^{-(\kappa_e+1)}. \quad (2)$$

κ_e is the electron index of superthermality and should be $\kappa_e > 1.5$. For higher values of κ_e, the kappa distribution in practice reduces to a Maxwellian distribution. Here $\theta_{e_\kappa} = \sqrt{\frac{\kappa_e-1.5}{\kappa_e}}\sqrt{2T_{e_\kappa}/m_e}$ is the most probable speed of kappa-distributed electrons, with the equivalent temperature T_{e_κ} in units of energy. v_{e_κ} and Γ represent the speed of the suprathermal electron and gamma function, respectively. The streaming speed of the suprathermal electron is represented by u_{0_κ}.

The plasma dispersion relation (Mace et al. 1998; Mace & Hellberg 2009) for this set of plasma can be written as

$$D(k,\omega) = 1 - \frac{\omega_{pe_w}^2}{k^2\theta_{e_w}^2}\acute{Z}(\zeta_{e_w}) - \frac{\omega_{pe_c}^2}{k^2\theta_{e_c}^2}\acute{Z}(\zeta_{e_c}) - \frac{\omega_{pe_\kappa}^2}{k^2\theta_{e_\kappa}^2}\acute{Z}(\kappa_e;\zeta_{e_\kappa}) - \frac{\omega_{pi}^2}{k^2\theta_i^2}\acute{Z}(\zeta_i). \quad (3)$$

In Equation (3), $\omega_{pe_w} = \sqrt{\frac{n_{e_w}e^2}{m_e\epsilon_0}}$, $\omega_{pe_c} = \sqrt{\frac{n_{e_c}e^2}{m_e\epsilon_0}}$, $\omega_{pe_\kappa} = \sqrt{\frac{n_{e_\kappa}e^2}{m_e\epsilon_0}}$, and $\omega_{pi} = \sqrt{\frac{n_ie^2}{m_i\epsilon_0}}$ are the plasma frequencies of warm, cold, suprathermal electrons, and ion species, respectively. $\theta_\alpha = v_{t\alpha}$ is the thermal speed of species α. Using the ion acoustic wave criteria, $\theta_i < \omega/k < \theta_{e_\kappa}, \theta_{e_w}, \theta_{e_c}$, the derivative of the plasma dispersion function can be approximated for lower-phase and higher-phase velocity limits as

$$\acute{Z}(\zeta_{e_w}) = -2 - i2\sqrt{\pi}\zeta_{e_w}\exp(-\zeta_{e_w}^2) + ..., \quad (4)$$

$$\acute{Z}(\zeta_{e_c}) = -2 - i2\sqrt{\pi}\zeta_{e_c}\exp(-\zeta_{e_c}^2) + ..., \quad (5)$$

$$\acute{Z}(\kappa_e;\zeta_{e_\kappa}) = -\left(\frac{2\kappa_e-1}{\kappa_e}\right) - i\frac{2\sqrt{\pi}\Gamma(\kappa_e)}{\sqrt{\kappa_e}\Gamma\left(\kappa_e-\frac{1}{2}\right)}\zeta_{e_\kappa} + ..., \quad (6)$$

$$\acute{Z}(\zeta_i) = \frac{1}{\zeta_i^2} + \frac{3}{2}\frac{1}{\zeta_i^4} - i2\sqrt{\pi}\zeta_i\exp(-\zeta_i^2) + ... \quad (7)$$

Assuming that only warm and suprathermal electrons drift, $\omega = \omega_r + i\gamma$, $|\gamma| \ll |\omega_r|$, and using $\zeta_{e_w} = \frac{\omega_r - ku_{0_w}}{k\theta_{e_w}}$, $\zeta_{e_c} = \frac{\omega_r}{k\theta_{e_c}}$, $\zeta_{e_\kappa} = \frac{\omega_r - ku_{0_\kappa}}{k\theta_{e_\kappa}}$, and $\zeta_i = \frac{\omega_r}{k\theta_i}$, we get the following dispersion relation:

$$D(k,\omega) = D_r(k,\omega) + iD_i(k,\omega) = 0. \quad (8)$$

The u_{0_w} is the streaming speed of the warm electron population, whereas $D_r(k,\omega)$ and $D_i(k,\omega)$ are the real and imaginary parts of the dispersion relation and are given as

$$D_r(k,\omega) = 1 + \frac{2\omega_{pe_w}^2}{k^2\theta_{e_w}^2} + \frac{2\omega_{pe_c}^2}{k^2\theta_{e_c}^2} + \left(\frac{\kappa_e-0.5}{\kappa_e}\right) \times\frac{2\omega_{pe_\kappa}^2}{k^2\theta_{e_\kappa}^2} - \frac{\omega_{pi}^2}{\omega_r^2}\left[1+\frac{3}{2}\frac{k^2\theta_i^2}{\omega_r^2}\right], \quad (9)$$

$$D_i(k,\omega) = \frac{\omega_r\omega_{pe_w}^2}{k^3\theta_{e_w}^3}2\sqrt{\pi}\left(1-\frac{u_{0_w}}{\omega_r/k}\right)\exp\left(-\frac{(\omega_r-ku_{0_w})^2}{k^2\theta_{e_w}^2}\right) + \frac{\omega_r\omega_{pe_c}^2}{k^3\theta_{e_c}^3}2\sqrt{\pi}\exp\left(-\frac{\omega_r^2}{k^2\theta_{e_c}^2}\right) + \frac{\omega_r\omega_{pe_\kappa}^2}{k^3\theta_{e_\kappa}^3}\frac{2\sqrt{\pi}\Gamma(\kappa_e)}{\sqrt{\kappa_e}\Gamma(\kappa_e-0.5)}\left(1-\frac{u_{0_\kappa}}{\omega_r/k}\right) + \frac{\omega_r\omega_{pi}^2}{k^3\theta_i^3}2\sqrt{\pi}\exp\left(-\frac{\omega_r^2}{k^2\theta_i^2}\right) + 2\frac{\gamma\omega_{pi}^2}{\omega_r^3}. \quad (10)$$

Equating $D_r(k,\omega) = 0$ yields

$$1 + \frac{1}{k^2\lambda_{De_w}^2} + \frac{1}{k^2\lambda_{De_c}^2} + \frac{1}{k^2\lambda_{De_\kappa}^2} - \frac{\omega_{pi}^2}{\omega_r^2}\left[1+\frac{3}{2}\frac{k^2\theta_i^2}{\omega_r^2}\right] = 0, \quad (11)$$

where $\lambda_{De_w} = \sqrt{\frac{\epsilon_0 T_{e_w}}{n_{e_w}e^2}}$, $\lambda_{De_c} = \sqrt{\frac{\epsilon_0 T_{e_c}}{n_{e_c}e^2}}$, and $\lambda_{De_\kappa} = \sqrt{\frac{\kappa_e-1.5}{\kappa_e-0.5}}\sqrt{\frac{\epsilon_0 T_{e_\kappa}}{n_{e_\kappa}e^2}}$ are the Debye lengths of warm, cold, and suprathermal electron species, respectively. Equation (11) can be written as

$$(1+k^2\lambda_{De}^2)\omega_r^4 - C_s^2k^2\omega_r^2 - \frac{3}{2}k^4C_s^2\theta_i^2 = 0, \quad (12)$$

where $\lambda_{De} = \sqrt{\frac{\epsilon_0 T_e}{n_e e^2}}$ and $C_s = \sqrt{T_e/m_i}$ with total electron density $n_e = n_{e_w} + n_{e_c} + n_{e_\kappa}$ and effective electron temperature

$$T_e = \frac{n_e T_{e_w}T_{e_c}T_{e_\kappa}}{n_{e_w}T_{e_c}T_{e_\kappa} + n_{e_c}T_{e_w}T_{e_\kappa} + n_{e_\kappa}\frac{\kappa_e-0.5}{\kappa_e-1.5}T_{e_w}T_{e_c}}.$$

If there are no cold and suprathermal electrons, then Equation (12) reduces to a simple thermal electron–ion plasma dispersion relation (Baumjohann & Treumann 1996). Equating $D_i(k,\omega) = 0$, the Landau damping or resonant wave–particle interaction rate can be approximated as

$$\gamma = \gamma_{e_w} + \gamma_{e_c} + \gamma_{e_\kappa} + \gamma_i, \quad (13)$$

where γ_{e_w}, γ_{e_c}, γ_{e_κ}, and γ_i are the Landau damping or growth rate due to warm, cold, suprathermal electron, and water ion

species, respectively. They are given as follows:

$$\gamma_{e_w} = -\sqrt{\pi}\,\omega_r^4\left[\frac{\omega_{pe_w}^2}{k^3\theta_{e_w}^3\omega_{pi}^2}\left(1-\frac{u_{0_w}}{\omega_r/k}\right)\times\exp\left(-\frac{(\omega_r-ku_{0_w})^2}{k^2\theta_{e_w}^2}\right)\right], \tag{14}$$

$$\gamma_{e_c} = -\sqrt{\pi}\,\omega_r^4\left[\frac{\omega_{pe_c}^2}{k^3\theta_{e_c}^3\omega_{pi}^2}\exp\left(-\frac{\omega_r^2}{k^2\theta_{e_c}^2}\right)\right], \tag{15}$$

$$\gamma_{e_\kappa} = -\sqrt{\pi}\,\omega_r^4\left[\frac{\omega_{pe_\kappa}^2}{k^3\theta_{e_\kappa}^3\omega_{pi}^2}\frac{\Gamma(\kappa_e)}{\sqrt{\kappa_e}\Gamma(\kappa_e-0.5)}\left(1-\frac{u_{0_\kappa}}{\omega_r/k}\right)\right], \tag{16}$$

$$\gamma_i = -\sqrt{\pi}\,\omega_r^4\left[\frac{1}{k^3\theta_i^3}\exp\left(-\frac{\omega_r^2}{k^2\theta_i^2}\right)\right]. \tag{17}$$

3. Result Analysis

For the result analysis, we used typical cometary plasma parameters (Madanian et al. 2016; Gunell et al. 2017a, 2017b). Specifically, $n_e = 1\times10^9\ \mathrm{m}^{-3}$, $T_{e_w} = 10\,\mathrm{eV}$, $T_{e_c} = 0.1\,\mathrm{eV}$, $T_{e_\kappa} = 100\,\mathrm{eV}$, and $T_i = 0.01\,\mathrm{eV}$. In order to explore the importance of cold and suprathermal electron populations, the analysis is carried out for the following three cases.

3.1. Warm and Cold Electron Populations

When there is no suprathermal electrons then $n_e = n_{e_w} + n_{e_c}$ and the effective electron temperature is

$$T_e = \frac{n_e T_{e_w} T_{e_c}}{n_{e_w} T_{e_c} + n_{e_c} T_{e_w}}.$$

In this case, the condition for current-driven ion acoustic instability is

$$\frac{u_{0_w}k}{\omega_r} > 1 + \frac{\omega_{pe_c}^2}{\omega_{pe_w}^2}\frac{\theta_{e_w}^3}{\theta_{e_c}^3}\exp\left(\frac{(\omega_r-ku_{0_w})^2}{k^2\theta_{e_w}^2}-\frac{\omega_r^2}{k^2\theta_{e_c}^2}\right) + \frac{\omega_{pi}^2}{\omega_{pe_w}^2}\frac{\theta_{e_w}^3}{\theta_i^3}\exp\left(\frac{(\omega_r-ku_{0_w})^2}{k^2\theta_{e_w}^2}-\frac{\omega_r^2}{k^2\theta_i^2}\right). \tag{18}$$

Let us first analyze the result in the absence of drift motion, i.e., $u_{0_w} = 0$. The phase speed of the ion acoustic wave increases by decreasing the cold electron density as shown in Figure 1(a).

The resonant wave–particle interaction rate due to the warm electrons decreases by increasing the cold electron density (Figure 1(b)). Figure 1(c) shows that the highest Landau damping due to the cold electron population is observed when n_{e_c} is 2% of the total electron density. A higher and smaller amount of cold electrons other than this critical value results in lower Landau damping. The resonant wave–particle interaction is mostly carried out by the cold electron population up to $k \sim 8.5\ \mathrm{m}^{-1}$, after which the resonant wave–ion interaction becomes dominant (Figure 1(d)). With drifting warm electrons, the damping rate of cold electrons and water ions remain unchanged, whereas the warm population imparts its energy to the wave and causes current-driven ion acoustic instability as seen in Figure 1(e). With a small amount of cold electrons, it is easier to excite the ion acoustic instability at relatively lower drift speed. For example, with $u_{0_w} = 5\times10^4\,\mathrm{m\,s}^{-1}$, the instability is seen for $n_{e_c} = 1\%$, 2% but $n_{e_c} = 10\%$ does not support the instability (Figure 1(e)).

3.2. Warm and Suprathermal Electron Populations

When there are no cold electrons then $n_e = n_{e_w} + n_{e_\kappa}$ and the effective electron temperature

$$T_e = \frac{n_e T_{e_w} T_{e_\kappa}}{n_{e_w} T_{e_\kappa} + n_{e_\kappa}\frac{\kappa_e-0.5}{\kappa_e-1.5}T_{e_w}}.$$

The current-driven ion acoustic instability condition in this case reads as

$$\frac{u_{0_w}k}{\omega_r} > 1 + \left(1-\frac{u_{0_\kappa}k}{\omega_r}\right)\frac{\omega_{pe_\kappa}^2}{\omega_{pe_w}^2}\frac{\theta_{e_w}^3}{\theta_{e_\kappa}^3}\frac{\Gamma(\kappa_e)}{\sqrt{\kappa_e}\Gamma(\kappa_e-0.5)} \times\exp\left(\frac{(\omega_r-ku_{0_w})^2}{k^2\theta_{e_w}^2}\right) + \frac{\omega_{pi}^2}{\omega_{pe_w}^2}\frac{\theta_{e_w}^3}{\theta_i^3} \times\exp\left(\frac{(\omega_r-ku_{0_w})^2}{k^2\theta_{e_w}^2}-\frac{\omega_r^2}{k^2\theta_i^2}\right). \tag{19}$$

In the absence of drifts, i.e., $u_{0_w} = u_{0_\kappa} = 0$, the phase speed of the wave does not change with the varying concentration of high-energy suprathermal electrons (Figure 2(a)). Therefore, the contributions to the damping rate from warm and kappa-distributed electrons only vary with the density (Figures 2(b), (c)). In this case, the warm electrons play a dominant role in the wave damping. The damping rate due to ions gets stronger than electrons around $k \sim 8\ \mathrm{m}^{-1}$ (Figure 2(d)). With $u_{0_w} = 1\times10^4\,\mathrm{m\,s}^{-1}$ and $u_{0_\kappa} = 0$, the growth rate of the current-driven ion acoustic instability falls as the density of suprathermal electrons increases, as shown in (Figure 2(e)). With $u_{0_\kappa} = 3.5\times10^4\,\mathrm{m\,s}^{-1}$ and $u_{0_w} = 0$, the elevated concentration of suprathermal electrons supports the instability ((Figure 2(f)).

3.3. Warm, Cold, and Suprathermal Electron Populations

In this case, the analysis of Section 3.1 is repeated in the presence of $n_{e_\kappa} = 10\%$ suprathermal electrons. The variation of ω, γ_{e_w}, γ_{e_c}, γ_{e_κ}, γ_i, and γ with respect to wavenumber showed no difference from previous results. Also, the analysis of Section 3.2 is repeated in the presence of $n_{e_c} = 2\%$ cold electrons. Quantitatively different but qualitatively similar results to those in Section 3.2 were obtained. In the presence of lower-energy cold electrons, relatively higher streaming speeds of warm and suprathermal electrons are required to excite the current-driven ion acoustic instability. These results are not shown here to avoid repetition.

Our results show that cold electrons significantly damped out the waves and suppressed instabilities. Based on these findings, it seems pertinent to argue that the sporadic observations of ion acoustic events in the cavity of comet 67P (Gunell et al. 2017a) could be due to the enhanced density of cold electrons. We also speculate that the short-lived low-frequency waves detected in the cavity (Madsen et al. 2018) were probably current-driven ion acoustic instabilities that were rapidly damped by the presence of too much cold electrons.

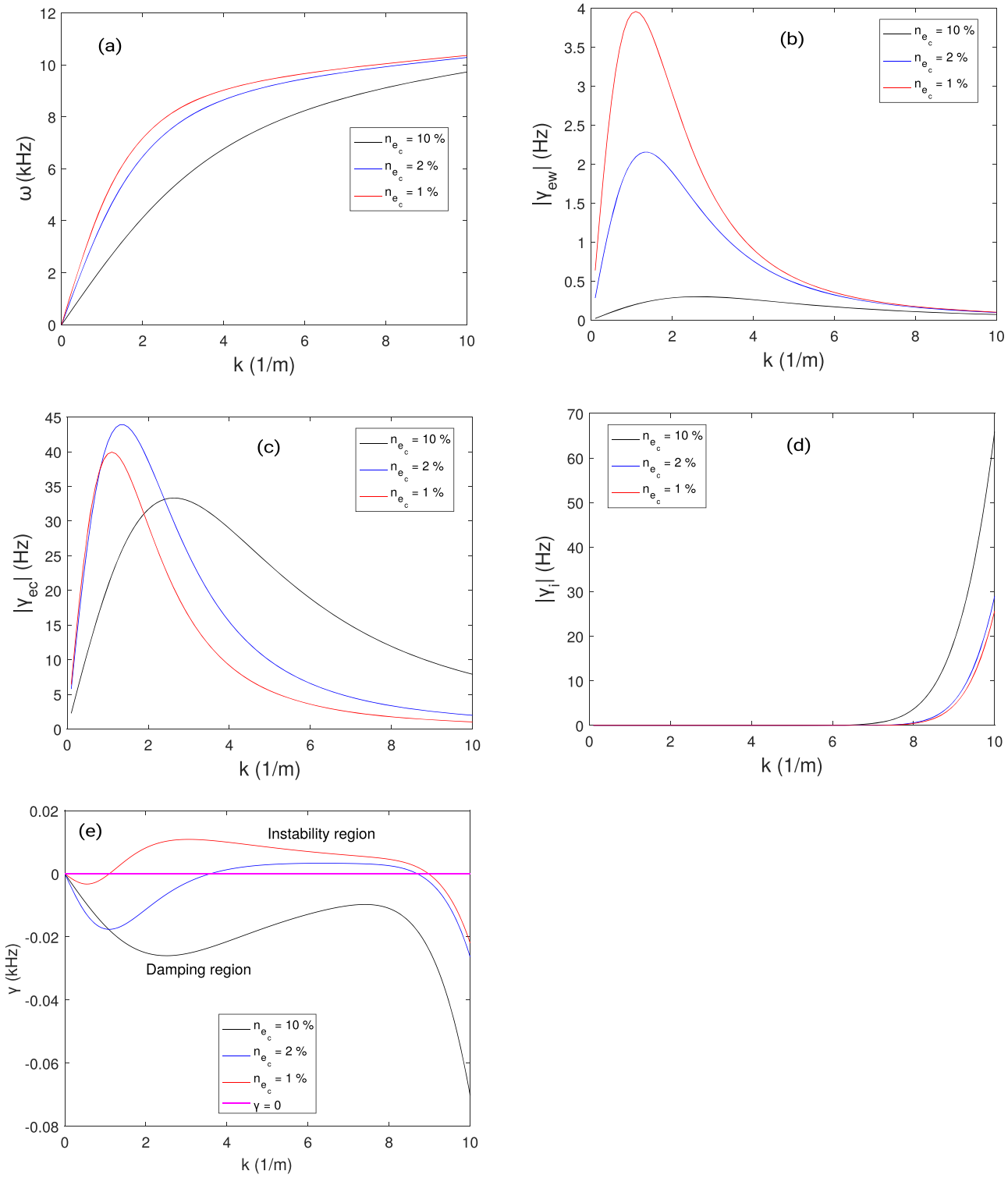

Figure 1. Variation of the ion acoustic wave properties with the varying densities of cold electron population. The properties are: (a) dispersion relation; the Landau damping rates due to the (b) warm and (c) cold electron populations, and (d) water ion species; and (e) the resonant wave–particle interaction rate with drifting warm electron population.

4. Conclusion

In conclusion, we developed a detailed kinetic model for investigating the ion acoustic wave dispersion and its resonance interaction with water ions and multiple electrons, i.e., cold, warm, and suprathermal electrons, plasma. Such types of plasma and ion acoustic waves have been recently observed by *Rosetta* at comet 67P/Churyumov–Gerasimenko. Our model results showed the highest Landau damping rate for smaller amounts ($n_{e_c} = 2\%$) of cold electrons. In the absence of cold electrons, the wave phase speed does not change by populating the high-energy suprathermal electron species, therefore the Landau damping rate of both warm and suprathermal electrons increases by increasing their respective densities. In case of

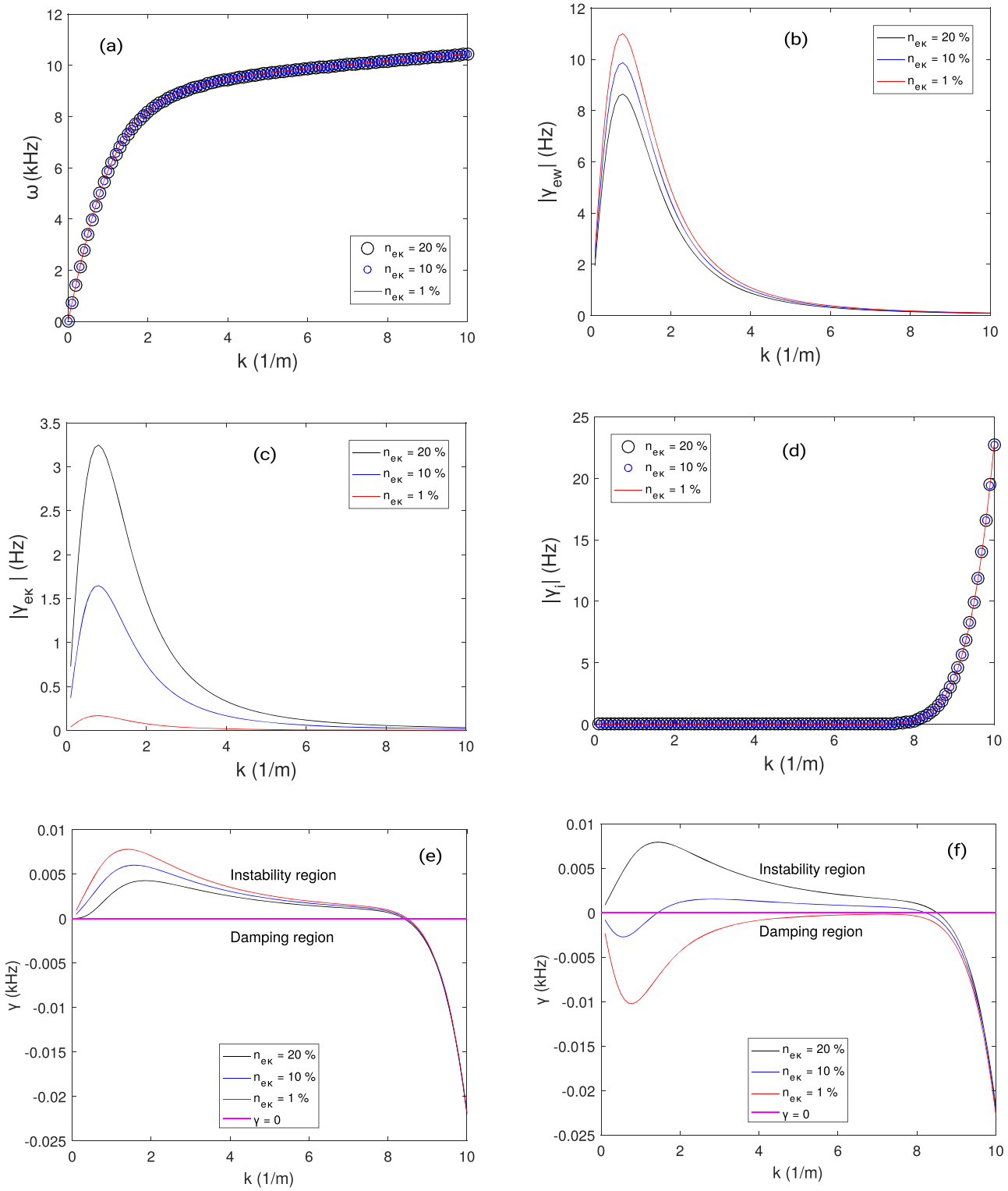

Figure 2. Variation of the ion acoustic wave properties with the varying densities of the suprathermal electron population. The properties are: (a) dispersion relation; the Landau damping rate due to the (b) warm and (c) suprathermal electron populations and (d) water ion species; and the resonant wave–particle interaction rate with the drifting (e) warm and (f) suprathermal electron populations.

drifting warm and stationary suprathermal electrons, the amplitude of the current-driven ion acoustic instability falls by increasing the density of suprathermal electrons. In the case of stationary warm and drifting suprathermal electrons, however, the elevated concentration of high-energy suprathermal electrons supports the instability. The lower density of cold electrons is found to support the current-driven ion acoustic instability at relatively lower drift speeds of the warm and suprathermal electron species. Future investigations of such plasma, in which one or more species are multi-distributed, could explore new types of plasma instabilities and their role in particle transport.

References

Baumjohann, W., & Treumann, R. A. 1996, Basic Space Plasma Physics (London: Imperial College Press, World Scientific)
Behar, E., Nilsson, H., Wieser, G. S., et al. 2016, GeoRL, 43, 1411
Broiles, T., Livadiotis, G., Burch, J., et al. 2016a, JGRA, 121, 7407
Broiles, T. W., Burch, J., Chae, K., et al. 2016b, MNRAS, 462, S312
Clark, G., Broiles, T., Burch, J., et al. 2015, A&A, 583, A24
Deca, J., Divin, A., Henri, P., et al. 2017, PhRvL, 118, 205101
Engelhardt, I. A., Eriksson, A. I., Vigren, E., et al. 2018, A&A, 616, A51
Eriksson, A. I., Engelhardt, I. A., André, M., et al. 2017, A&A, 605, A15
Gilet, N., Henri, P., Wattieaux, G., Cilibrasi, M., & Béghin, C. 2017, RaSc, 52, 1432
Gunell, H., Goetz, C., Eriksson, A., et al. 2017a, MNRAS, 469, S84
Gunell, H., Nilsson, H., Hamrin, M., et al. 2017b, A&A, 600, A3
Karlsson, T., Eriksson, A. I., Odelstad, E., et al. 2017, GeoRL, 44, 1641
Mace, R., Hellberg, M., & Treumann, R. 1998, JPlPh, 59, 393
Mace, R. L., & Hellberg, M. A. 2009, PhPl, 16, 072113
Madanian, H., Cravens, T., Rahmati, A., et al. 2016, JGRA, 121, 5815
Madsen, B., Wedlund, C. S., Eriksson, A., et al. 2018, GeoRL, 45, 3854
Nilsson, H., Stenberg Wieser, G., Behar, E., et al. 2015, Sci, 347, aaa0571
Oya, H., Morioka, A., Miyake, W., Smith, E. J., & Tsurutani, B. T. 1986, Natur, 321, 307
Scarf, F. L., Coroniti, F. V., Kennel, C. F., et al. 1986, Sci, 232, 377